Chemistry Faculty Research and Publications   Chemistry, Department of

10-2-2020

Solving Complex Eigenvalue Problems on A Quantum Annealer with Applications to Quantum Scattering Resonances

Alexander Teplukhin
Los Alamos National Laboratory

Brian K. Kendrick
Los Alamos National Laboratory

Dmitri Babikov
Marquette University, dmitri.babikov@marquette.edu

Solving Complex Eigenvalue Problems on A Quantum Annealer with Applications to Quantum Scattering Resonances

Alexander Teplukhin
Theoretical Division (T-1, MS B221), Los Alamos National Laboratory, Los Alamos, New Mexico
Brian K. Kendrick
Theoretical Division (T-1, MS B221), Los Alamos National Laboratory, Los Alamos, New Mexico
Dmitri Babikov
Department of Chemistry, Marquette University, Milwaukee, Wisconsin

Abstract

Quantum computing is a new and rapidly evolving paradigm for solving chemistry problems. In previous work, we developed the Quantum Annealer Eigensolver (QAE) and applied it to the calculation of the vibrational spectrum of a molecule on the D-Wave quantum annealer. However, the original QAE methodology was applicable to real symmetric matrices only. For many physics and

chemistry problems, the diagonalization of complex matrices is required. For example, the calculation of quantum scattering resonances can be formulated as a complex eigenvalue problem where the real part of the eigenvalue is the resonance energy and the imaginary part is proportional to the resonance width. In the present work, we generalize the QAE to treat complex matrices: first complex Hermitian matrices and then complex symmetric matrices. These generalizations are then used to compute a quantum scattering resonance state in a 1D model potential for $O + O$ collisions. These calculations are performed using both a software (classical) annealer and hardware annealer (the D-Wave 2000Q). The results of the complex QAE are also benchmarked against a standard linear algebra library (LAPACK). This work presents the first numerical solution of a complex eigenvalue problem of any kind on a quantum annealer, and it is the first treatment of a quantum scattering resonance on any quantum device.

1 Introduction

Quantum computers are expected to supersede classical computers one day and scientists around the world are working hard to bring that day closer. A number of quantum computing models and physical platforms[1,2] to realize reliable qubits are under investigation and it is still not clear what model and platform are going to win the competition. In the meantime, scientists are also pursuing the development of quantum algorithms[3,4] for current Noisy Intermediate-Scale Quantum (NISQ) devices,[5] before true universal quantum computers become available. The applications of quantum computers and quantum algorithms are limitless and theoretical chemistry is one of the fields that will significantly benefit from them.[6–8]

Currently, the two most dominant quantum computing models are gate-based quantum computing and adiabatic quantum annealing.[6] In the first model of computation, a sequence of quantum gates (*i.e.*, reversible unitary transformations) is applied to a number of qubits and the states of all qubits are measured at the end. The model has gained widespread popularity because it gives full control over the qubits and computation itself. In the literature, the Variational Quantum Eigensolver (VQE)[9–11] is one of the most popular algorithms implemented on gate-based quantum computers. The solver was successfully applied to the calculation of the electronic ground state energy of a molecule – one of the most important fundamental problems in computational chemistry.

Adiabatic quantum annealing is another, probably less popular model of quantum computation. In this model, the computation is based on the slow continuous transformation of an initial (easy-to-prepare) Hamiltonian into a final (target) Hamiltonian. The ground state of the initial Hamiltonian adiabatically becomes the ground state of the final Hamiltonian. In practice, a given problem must be formulated as an Ising problem or equivalently a Quadratic Unconstrained Binary Optimization (QUBO) problem. Specifically, a QUBO solver finds the minimum of the QUBO function $x_Q^T x$ (called the objective function), where Q is a matrix describing the problem and x is a binary string (string of zeros and ones). At the minimum, the optimal solution string $x = x_{\text{opt}}$ is obtained. If a problem can be converted into a QUBO problem, then it can be solved on an annealer, otherwise it cannot be solved on that type of quantum device. This significantly decreases the applicability of quantum annealing, as not every problem is convertible. In comparison to the gate-based quantum computers, quantum annealers have a much larger number of qubits, but this should not be misunderstood, as those qubits are loosely-connected. In order to emulate an all-to-all connectivity (*i.e.*, full coupling between all of the qubits),

one needs to sacrifice a large portion of the qubits for chain construction which effectively reduces the number of qubits from 2048 to just 64 on the D-Wave 2000Q.[12] Interestingly, the two models of computation: gate-based and adiabatic quantum annealing have been shown to be formally equivalent (at least for ideal quantum devices).[13]

Due to the limited applicability of quantum annealers, the number of studies where this type of quantum device is used to solve chemistry problems is quite small. For example, there are only two studies where the electronic Hamiltonian is mapped to a quantum annealer. The method of the first paper[14] converts all Pauli operators of the second-quantized Hamiltonian to the σ_z operator (the only operator implemented in the current generation of D-Wave annealers) and makes multiple replicas of basis functions to mimic basis function weights. The method was later implemented on a real D-Wave annealer to find the ground state energy of H_2 and LiH.[15] The second approach[16] is based on the fact that if one writes the expectation value of the second-quantized Hamiltonian in terms of Bloch sphere angles, then the expression becomes a sum of products of primitive trigonometric functions. The quadrant of each Bloch angle can be stored using one or two binary variables. The function of these binary variables is then optimized on a quantum annealer while the remaining angles within the $[0, \pi/2]$ range are optimized classically.

The Quantum Annealer Eigensolver (QAE)[17] can also be used to solve chemistry problems. For example, previously, the method has been applied to compute the vibrational spectrum of a molecule.[17] The QAE is a general-purpose eigenvalue solver that runs on the D-Wave quantum annealer. If a problem can be formulated as eigenvalue problem, then the QAE can be used to solve that problem. The method is Hamiltonian and basis agnostic as only a matrix needs to be provided.

As a matrix-based method, the QAE inherits all intrinsic limitations of the matrix representation, such as exponential scaling with the problem size for the matrices constructed using direct product basis sets. A smarter choice of the basis potentially may improve the scaling. However, other methods of solving the eigenvalue problem on existing annealers (*e.g.*, for the electronic structure[14,16]) scale exponentially as well. This is a limitation of the current generation of D-Wave annealers, which currently do not implement non-stoquastic Hamiltonians, needed to realize a better scaling.[18]

Thus, the primary goal of the QAE[17] and the present study is to show how one can map a fundamental physics or chemistry variational (eigenvalue) problem onto the existing quantum annealer hardware or equivalently an Ising Hamiltonian, and demonstrate it on available quantum devices. While the long-term goals of quantum computing are to realize a quantum advantage and ultimately an exponential speed-up, these goals are beyond the scope of the current study and will require more advanced quantum algorithms and hardware.

Specifically, in the present study, we generalize the QAE to solve complex matrices, both Hermitian and complex symmetric. The new methodology is then applied to compute quantum scattering resonances. The real part of a complex eigenvalue is the resonance energy, while the imaginary part is related to the resonance width Γ via: $E = E_{\text{res}} + (-\Gamma/2)i$. The lifetime of a resonance is the inverse of the resonance width, $\tau = \hbar/\Gamma$. We apply the complex QAE to a one-dimensional (1D) O + O scattering problem using a simplified interaction potential to facilitate calculations. The QAE is run on both a

classical annealer and a hardware quantum annealer (the D-Wave 2000Q). Both sets of results are benchmarked against a standard (classical) numerically exact linear algebra library (LAPACK).[19]

To the best of our knowledge, this work is the first time when a complex eigenvalue problem is solved on a quantum annealer, and it is the first treatment of a quantum scattering resonance on any quantum device.

2 Methodology

The Quantum Annealer Eigensolver (QAE)[17] is based on the min-max theorem which states (in the simplest formulation) that for a $n \times n$ Hermitian matrix A the smallest (largest) eigenvalue is equal to the minimum (maximum) of the Rayleigh–Ritz quotient

$$R_A = (Av,v)/(v,v) \quad (1)$$

or

$$R_A = (Av,v) \quad (2)$$

if the vector v is normalized. The vector $v_{\min}$ ($v_{\max}$) for which this minimum (maximum) is reached is the associated eigenvector. One may notice that R_A is quite similar to the QUBO expression $x_Q^T x$, which is what the D-Wave quantum annealer optimizes. First, we will consider real symmetric A and then generalize to the complex cases below. For the real case, a matrix of real numbers is common to both expressions: A for the quotient in eqn (1) and Q for the QUBO problem. However, v is a vector of real numbers, whereas x is a vector of binary values. To map the first to the second, we use a fixed-point representation for the elements of v. In this encoding, an element v_α is represented using K binary variables or qubits $q_i^\alpha, 1 \leq i \leq K$, so that each qubit contributes a fraction (1/2, 1/4, *etc.*) to the v_α and one more qubit is responsible for the sign, see eqn (10) in the Appendix. The products of powers-of-two and the matrix elements of A give the matrix elements of Q. In this way, we have mapped the eigenvalue problem onto the QUBO problem required for running on a quantum annealer.

After the mapping is established, one also needs to consider adding a normalization constraint to the QUBO, because the optimal $v_{\min}$ represented by x might be a zero vector (*i.e.*, the trivial solution $v = \mathbf{0}$). In order to avoid that, we have to augment the QUBO function with some constraint to encourage $\|v\| = 1$. The most obvious way is to add a term $\lambda(\|v\| - 1)^2$ to the QUBO with some penalty parameter λ, but this will make the QUBO biquadratic in q_i^α and unmappable to the D-Wave annealer. There is a procedure to handle terms beyond quadratic, but it requires adding more constraints which increases the total number of unknown penalties (or constraint multipliers). Instead, we suggest dropping the second power in the added constraint to keep the QUBO quadratic in q. In practice, the usage of a linear form of the constraint does not cause problems, see Results and discussion section for additional details concerning the constraint form. The constant shift λ can also be dropped once the constraint is linear. Thus, the final objective function is given by

$$F(v) = (v,Av) + \lambda \cdot (v,v). \quad (3)$$

While eqn (3) looks like a Lagrangian and is usually tackled with the Lagrange multiplier method (for example, see the standard Hartree–Fock method[20]), here we will be optimizing $F(v)$ for multiple values of λ, chosen iteratively (see below). Now, the $v \rightarrow q$ mapping discussed above can be used to construct the corresponding QUBO function $F_Q(q)$ that can then be minimized on a quantum annealer. Please see eqn (11) and (12) in the Appendix for the explicit form of $F_Q(q)$.

The normalization penalty λ balances two things in the QUBO function $F(v)$: the expectation value and the norm. One has to find a "sweet spot", such that the normalization constraint is satisfied and the expectation value is the lowest possible. With the linear form of the normalization constraint there is not much of an actual constraint to satisfy, strictly speaking. However, it does provide a way to avoid the trivial solution and encourage a non-zero norm. A small λ causes the norm to be neglected, while a large λ causes the Hamiltonian contribution to be neglected (relative to the norm). Thus, the optimal λ_{opt} is located somewhere in between. In the past,[17] we did a simple scanning in λ, but that required specifying the λ-range to scan. Instead, the current version of the QAE iteratively searches for the best λ_{opt} without any additional input from the user.

The positive and negative values of the maximum matrix element of A serve as the range limits where λ_{opt} is searched. On each λ iteration, the QUBO is minimized and the vector v is constructed from the binary string q. The vector v is then used to evaluate the expectation value (v, Av). The expectation value can be used to guide the next choice of λ. However, for inaccurate noisy QUBO solvers (see below), the expectation value fluctuates on each run. Thus, it is not a reliable measure to guide the next choice for λ. Instead, we base our search on the type of solution, trivial or non-trivial. The λ_{opt} is always located around a "phase-transition" point – on the edge between trivial and non-trivial solution areas. Thus, the QAE iteratively shrinks the search range, so that the solution on the left end is always non-trivial, whereas the solution on the right end is always trivial. For each λ the expectation value (v, Av) is stored and the smallest one is returned to the user once the iterations stop.

Currently, the QAE has two stopping criteria. One tracks how much the expectation value changes and stops the search if the recent changes are smaller than a user specified tolerance. The other condition occurs simply when the λ -search range shrinks to a single point. The latter one guaranties that the algorithm will eventually stop even when an inaccurate noisy QUBO solver is used.

Since the number of qubits required to obtain reliable results is much larger than the number of fully-connected logical qubits on the D-Wave annealer (64 for the D-Wave 2000Q), the QAE uses an intermediate (interface) software *qbsolv*.[21] The *qbsolv* enables the treatment of large QUBO problems. On each internal iteration, the *qbsolv* sorts the QUBO variables of a large QUBO in order of importance, splits the problem into subQUBOs of the size 64 qubits, minimizes each chunk separately, appends the resulting binary strings and refines the whole solution classically. The subQUBOs can be minimized either classically using a Tabu search algorithm or on a D-Wave quantum annealer. In this way, the QAE has two modes of operation: classical and hardware (which control how *qbsolv*'s subQUBOs are minimized).

While being a great tool to solve large QUBO problem, the *qbsolv* is noisy. Running it many times for the same QUBO problem gives different results on each run, independent of how the subQUBOs are

solved (*i.e.*, either classically or on the D-Wave annealer). This not only leads to fluctuating eigenvalues, but also limits a number of ways in which λ can be searched. For example, one cannot simply use gradient-based methods to find λ_{opt}.

The QAE algorithm can also be used to compute more than one eigenpair (*i.e.*, the excited quantum states). The *k*th eigenpair is found by repeating the whole procedure for a modified matrix

$$A' = A + \sum_{i=0}^{k-1} S_i(v_i \otimes v_i), \qquad \text{(4)}$$

where $\otimes$ denotes the outer product and the multipliers S_i shift the previously computed eigenpairs higher in the spectrum. The S_i should be large enough so that the next eigenpair of interest is the minimum energy solution of A'. In the current implementation they are set equal to the maximum matrix element multiplied by 16. However, other multipliers such as 2, 4, 8 have also worked well. A more robust technique for choosing the S_i values could be investigated but this is not our present focus.

2.1 Complex Hermitian matrices

In the complex case, both the given matrix *A* and its eigenvectors *c* are complex. This means that twice the number of qubits are needed to encode the problem of the same size ($n \times n$) than for the real case. One half of the qubits encodes the real part of an eigenvector c^{Re} and the other half encodes the imaginary part c^{Im}. As shown in the Appendix (see eqn (13) and (14)) each (α, β) term of the objective function $F(c)$ is now a complex number. However, due to the Hermitian property of *A*, the sum of two terms that have their indices exchanged (*i.e.*, (α, β) with (β, α)) gives a real number (see eqn (15)). Since the diagonal terms (α, α) are purely real for a Hermitian matrix, the whole objective function $F(c)$ and the resulting QUBO remain real. This is fortunate since the D-Wave annealers optimize real QUBOs only. A real objective function $F(c)$ is expected for Hermitian matrices since both components of $F(c)$, the expectation value (c, Ac) and the norm (c, c), have to be real. Thus, there are no changes to the fundamental algorithm of the QAE for the complex Hermitian case, other than doubling the qubit count and carefully tracking real and imaginary parts of the complex numbers involved. The final objective function is given by

$$F_{herm}(c) = (c, Ac) + \lambda \cdot (c, c) \qquad \text{(5)}$$

2.2 Complex symmetric matrices

The extension of the QAE to complex symmetric matrices is not as elegant as for the real and complex Hermitian matrices. This is due to the fact that both $F(c)$ and resulting QUBO are not real anymore. The sum of the (α, β) and (β, α) terms in $F(c)$ has an imaginary component, which replaces some of the real-valued terms in the similar expression for Hermitian matrices, see eqn (16). Generally speaking, the traditional variational method is not applicable in the complex symmetric case, because the eigenvalues are complex $E = E^{Re} + iE^{Im}$ and minimizing only the real part will not suffice. However, for the quantum scattering problem, we are interested in the lowest lying bound and quasi-

bound (resonance) states which have the smallest energy E^{Re} and smallest width $\Gamma = -2E^{\text{Im}}$. This means that the complex eigenvalues of interest are variational in the sense that they must have both small real and small imaginary parts. In a typical 1D scattering problem, all ro-vibrational states until the dissociation threshold are bound states with purely real eigenvalues (*i.e.*, they have zero width or infinite lifetime). The quasi-bound (resonance) states which lie above the dissociation threshold and are trapped behind the centrifugal barrier (and also include some states above the barrier energy) have complex eigenvalues with a finite width that increases with increasing energy. Examples of this correlation can be found in the literature, see Fig. 4 in ref. 22 (Lennard-Jones potential with centrifugal term) and Tables 1, 2 and 4 in ref. 23 (double barrier symmetric potentials). That is, the lifetime τ decreases with increasing resonance energy due to enhanced tunneling through the barrier. At very high energies above the barrier, the solutions approach the continuum states which have infinite width (*i.e.*, zero lifetime). Thus, at least for the complex symmetric matrices generated for quantum scattering problems, the QAE must be augmented with another constraint to minimize the imaginary part or width $\Gamma = -2E^{\text{Im}}$. Since the width is a positive number and we are trying to minimize it, the addition of the real valued term $(-2E^{\text{Im}})$ in the $F(c)$ is sufficient. The expression for E^{Im} in terms of the matrix and vector elements is given in the Appendix (see eqn (17)).

Similar to the normalization constraint, the new constraint on Γ has its own penalty γ. As before, the role of the new penalty factor is to balance components in the objective function and QUBO. Together, the two penalties, λ and γ, are used to balance three components of the whole expression: energy, norm and width. As a result, the search for the optimal weights, λ_{opt} and γ_{opt}, makes the complex symmetric QAE more expensive than the real and Hermitian versions. In practice, we found that the 2D search can be reduced to semi-2D by letting the λ penalty contribute to the Γ constraint, resulting in a $\lambda\gamma(-2E^{\text{Im}})$ form of the new constraint. The QUBO optimization in λ is now performed for multiple γ values.

Unfortunately, the proposed changes discussed above were not sufficient. After examining the QUBO terms, eqn (16) in the Appendix, one can see there are only $c_\alpha^{\text{Re}} c_\beta^{\text{Re}}$ and $c_\alpha^{\text{Im}} c_\beta^{\text{Im}}$ products, but there are no cross-terms $c_\alpha^{\text{Re}} c_\beta^{\text{Im}}$ or $c_\alpha^{\text{Im}} c_\beta^{\text{Re}}$. This means that the real and imaginary parts are independent and uncoupled. In contrast, for the Hermitian case the cross-terms are naturally included as part of the energy minimization and, as shown in the Appendix eqn (18) and (19), are responsible for the "angular repulsion" between the vector elements. With these terms added, the optimization is encouraged to explore the full 2π range of the complex phase and the complex symmetric QAE becomes stable, giving reasonable energies and widths. Thus, the final objective function for the complex symmetric QAE is given by

$$F_{\text{csym}}(c) = (c, Ac) + \lambda \cdot (c, c) - \lambda\gamma 2E^{\text{Im}} - \lambda\gamma' X(c) \quad (6)$$

where $X(c)$ contains all of the cross-terms from the Hermitian case (see eqn (18) in the Appendix). The new γ' weight is analogous to the γ weight introduced above for the imaginary constraint. It balances the relative contribution of the $-X(c)$ constraint with the other terms in eqn (6). The QUBO optimization of the final form of the functional given in eqn (6) with respect to λ is now performed for multiple γ and γ' values to determine the overall optimal complex symmetric eigenvalue solution. The

addition of the $-2E^{\text{Im}}$ and $-X(c)$ constraints does not affect the final computed energies similar to the normalization constraint.

3 Results and discussion

The new complex QAE methodology is applied to the calculation of both bound and quasi-bound (resonance) states of molecular oxygen O_2. The focus of the present work is to demonstrate the new capabilities of QAE. Thus, we use a simplified 1D model for O_2 where the depth of the O_2 potential well is artificially decreased in order to reduce the number of bound states to just one or two. The oxygen molecule is also rotationally excited to $j = 6$ which gives rise to a small centrifugal barrier that supports at least one quasi-bound state. The traditional approach for computing the quasi-bound (resonance) spectrum is to add a Complex Absorbing Potential (CAP) to the Hamiltonian. The Hamiltonian matrix is constructed using a suitable basis and the matrix is diagonalized to obtain the complex eigenvalues and eigenvectors. In the present work, we use two different basis sets and absorbing potentials with two different O_2 model potentials. One model leads to a Hermitian matrix and the other model gives a complex symmetric matrix. Thus, with these two model problems we can demonstrate both the Hermitian and complex symmetric versions of the new complex QAE methodology.

The 1D model problem is given by the Schrödinger equation

$$\left[-\frac{h^2}{2\mu}\frac{\partial^2}{\partial r^2} + \frac{h^2 j(j+1)}{2\mu r^2} + V(r) + V_{\text{abs}}(r) \right] \Psi(r) = E\Psi(r) \tag{7}$$

where μ is the reduced mass of O_2, r is the internuclear distance of O_2, j is the rotational quantum number, $V(r)$ is the O_2 interaction potential, $V_{\text{abs}}(r)$ is the absorbing potential, $\psi(r)$ is the wave function and E is the energy. The Hamiltonian operator (H) consists of the terms in the brackets acting on $\psi(r)$ on the left hand side of eqn (7) (*i.e.*, $H\psi(r) = E\psi(r)$). The interaction potential is chosen to be a standard Morse potential given by $V(r) = D_e\{\exp[-b(r - r_0)] - 2\exp[-b(r - r_0)]\}$ where D_e, b, and r_0 are parameters specified below. Two forms of the absorbing potential (V_{abs}) are utilized, a real quadratic potential

$$\begin{aligned} V_{\text{rap}}(r) &= \eta(r - r_c)^2 \; (r \geq r_c) \\ &= 0 \; (r \geq r_c) \end{aligned} \tag{8}$$

and a complex (purely imaginary) quadratic potential

$$\begin{aligned} V_{\text{cap}}(r) &= i\eta(r - r_c)^2 \; (r \geq r_c) \\ &= 0 \; (r < r_c) \end{aligned} \tag{9}$$

where η is the potential strength and r_c is its origin.

In the Hermitian model, the real absorbing potential of eqn (8) (with $\eta = 0.01$ and $r_c = 8.5a_0$) is used in eqn (7). The wave function $\psi(r)$ in eqn (7) is expanded using a complex Fourier basis given by

$$\Psi_j(r) = \sum_{m=-m_{max}}^{+m_{max}} c_m^j \exp(im\phi)/\sqrt{2\pi}$$

where $\phi_k = 2\pi k/n$, k is an integer labeling the kth grid point, and $n = 2m + 1$ denotes the total number of grid points. The grid in r is defined as: $r_k = r_{mid} + \phi_k dr$ where $dr = (r_f - r_i)/2\pi$ and r_i, r_f and r_{mid} denote the initial, final and midpoint of the grid. The grid parameters used in the Hermitian model are $r_i = 1.5a_0$, $r_f = 9.5a_0$, and $r_{mid} = 5.5a_0$. The complex expansion coefficients c_m^j are the eigenvectors. These are computed by diagonalizing the Hamiltonian matrix (H) which when evaluated in the complex Fourier basis is a Hermitian matrix. In order to keep the problem size small for QAE so that it fits on the existing quantum hardware (*e.g.*, the D-Wave annealer), we chose a small basis $m = 10$ which gives $n = 21$ grid points and a Hermitian matrix of size 21×21. A discretization with $K = 10$ qubits was used which results in a QUBO of size 210×210. To keep the problem size manageable, we also chose the positions of the absorbing potential wall to be as close as possible to the barrier, $r_c = 8.5a_0$. The dynamic range of the Hamiltonian matrix was also reduced by setting all matrix elements with absolute value larger than $E_{max} = 200$ cm^{-1} equal to E_{max}. This avoids wasting "precious" qubits in resolving the large matrix elements associated with the repulsive regions of the potential (we chose E_{max} large enough so not to significantly affect the low-lying eigensolutions of interest).

The true 1D potential for O_2 contains too many bound states (even with the centrifugal component added), which causes the QAE to do a lot of work before it can reach the first resonance state above the threshold. The QAE performs spectrum transformations using the previously computed low-energy states, as was explained earlier (see eqn (4)). This not only takes time, but also introduces noise (from the *qbsolv*) to the transformed matrices A', which may in turn corrupt high-energy solutions. Since the focus of the present work is to compute quasi-bound states, we artificially lowered the well depth of our O_2 model potential so that it supports only one or two bound states. For the Hermitian model, the Morse parameters for O_2 were chosen as $D_e = 200$ cm^{-1}, $b = 2.5836$, and $r_0 = 2.28189a_0$ (we note that the b and r_0 values are the correct values for O_2 and were unchanged, only the D_e was reduced from its true value of 44, 457.26 cm^{-1}). The corresponding model potential curve $V(r)$ is plotted in Fig. 1 (the thick black curve). This choice of Morse parameters together with $j = 6$ supports two bound states and one quasi-bound state (a shape resonance trapped behind the broad centrifugal barrier).
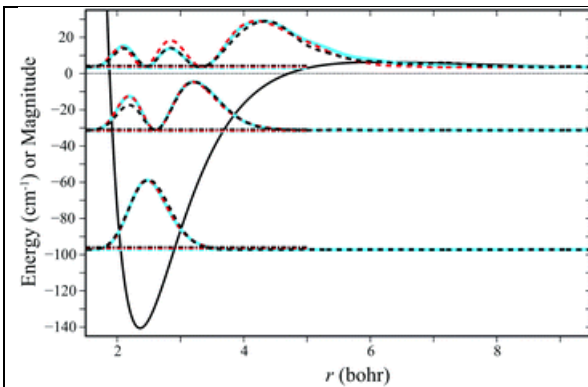

Fig. 1 Application of the Hermitian QAE to the calculation of bound and resonance states. Two bound states and one resonance were calculated in a model O_2 potential for $j = 6$ (black curve). The model Hamiltonian was diagonalized using LAPACK (blue), and the QAE in both classical (dashed red)

and hardware (D-Wave, dashed black) modes. The wave functions of all three methods are close to each other. The differences in state energies (horizontal dashed lines) are small (see Table 1).

The results of using the Hermitian QAE are shown in Fig. 1. For comparison, we calculated all three states using a standard numerical diagonalization library (LAPACK)[19] plotted in solid blue. The QAE results in classical mode are plotted in dashed red, and the QAE results in hardware mode on the D-Wave annealer are plotted in dashed black (thinner line). As one can see, there is not much difference between the three methods. Thus, the Hermitian QAE is working well for the calculation of both bound and resonance state energies and wave functions. The energies are all collected in Table 1. The optimal normalization penalty, determined iteratively, for each of the three states is $\lambda_{\text{bound1}} = 90.625$, $\lambda_{\text{bound2}} = 31.25$, and λ res $= -7.53326$, respectively. The eigenvectors computed using LAPACK and QAE were found to agree up to an overall arbitrary phase. The QAE eigenvectors had a different phase on each run, which nicely demonstrates a property of Hermitian matrix eigenvectors – the arbitrariness of the phase. It seems that the *qbsolv* noise ultimately determines the phase, rather than the less-influential hardware noise. In contrast, the LAPACK eigenvectors had the same phase on each run.

Table 1 The Hermitian bound and resonance state energies (cm^{-1}) computed using LAPACK, QAE in classical mode (QAE Cl.) and QAE in hardware mode (QAE Hw.)

State	LAPACK	QAE Cl.	QAE Hw.
Bound #1	−97.36	−96.44	−95.73
Bound #2	−32.00	−31.48	−30.73
Resonance	2.85	3.94	4.46

For the complex symmetric matrix model, the imaginary absorbing potential of eqn (9) (with $\eta = 0.005$ and $r_c = 13.0a_0$) is used in eqn (7). The wave function $\psi(r)$ in eqn (7) is expanded using real valued particle-in-a-box basis functions:

$$\Psi_j(r) = \sqrt{2/L} \sum_{m=1}^{m_{\text{max}}} c_m^j \sin(m\pi r/L)$$

where L is the width of the box $L = r_f - r_i$. The grid parameters used in the complex symmetric model are $r_i = 1.5a_0$ and $r_f = 13.5a_0$. The size of the basis set was $m_{\text{max}} = 20$ which gives a 20×20 dimensional complex symmetric matrix. A discretization of $K = 10$ qubits was used which results in a QUBO of size 200 × 200. For the complex symmetric model, the Morse parameter $D_e = 125$ cm^{-1} was chosen for O_2 (the b and r_0 are the same as in the Hermitian model). The corresponding potential curve $V(r)$ is plotted in Fig. 2 (the thick black curve). The smaller D_e value together with $j = 6$ supports one bound state and one quasi-bound (resonance) state. As was done for the Hermitian case, the dynamic range of the Hamiltonian matrix was reduced by setting all matrix elements with absolute value larger than $E_{\text{max}} = 75$ cm^{-1} equal to E_{max}.
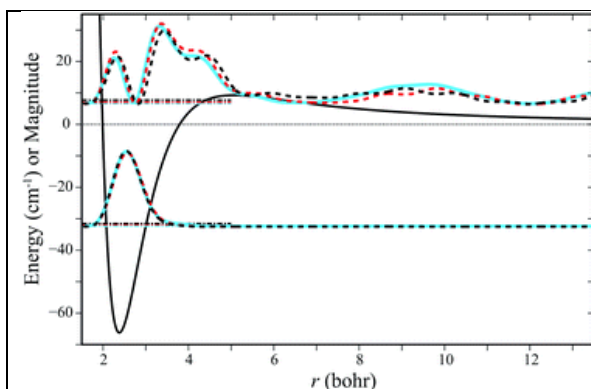
Fig. 2 Application of the complex symmetric QAE to the calculation of bound and resonance states. One bound and one resonance state were calculated in a model O_2 potential for $j = 6$ (black solid curve). The same complex symmetric matrix was solved using LAPACK (blue) and the QAE in both classical (dashed red) and hardware (D-Wave, dashed black) modes. The wave functions of all three methods are close to each other. The energies of both states computed using the three methods are almost the same (horizontal dashed lines).

The QUBO optimization in the QAE with respect to λ in eqn (6) was repeated on a 9 × 9 grid for a total of 81 values of the two new penalties γ and γ'. Specifically, each penalty was discretized on a grid of 9 values decreasing by a factor of two each time: 0.05, 0.025, 0.0125 0.00625, *etc.* In the present problem, only positive values of γ and γ' need be considered. The optimal values for these penalties were determined by running QAE ten times at each of the 81 values of γ and γ'. The real part of the QAE energy eigenvalue was averaged over the ten runs at each point and the point with the lowest average energy value was chosen. This procedure is repeated for each of the eigensolutions. The optimal γ and γ' for the bound and excited states were determined to be ($\gamma_{\text{bound}} = 7.8125 \times 10^{-3}, \gamma_{\text{bound}'} = 1.5625 \times 10^{-2}$) and ($\gamma^{\text{res}} = 7.8125 \times 10^{-3}, \gamma_{\text{res}'} = 0.25$), respectively. The optimal normalization penalty for each state, determined iteratively, is $\lambda_{\text{bound}} = 29.301453$ and $\lambda_{\text{res}} = -7.983398$.

Fig. 2 shows the QAE results for the complex symmetric matrix. Again the matrix was diagonalized using three methods: a traditional LAPACK diagonalization (blue) and the QAE in both classical (dashed red) and hardware (dashed black) modes. As with the Hermitian matrices, the differences in the energy and wave function computed using the three methods are very small. However, these new calculations treat the imaginary component of the energy explicitly and therefore provide the lifetime of the resonance. In contrast, the Hermitian approach gives only the real part of the eigenvalue (*i.e.*, the resonance energy but no resonance lifetime). The complex symmetric energies and lifetimes are collected in Table 2.

Table 2 The complex symmetric bound and resonance state energies (cm^{-1}) computed using LAPACK, QAE in classical mode (QAE Cl.) and QAE in hardware mode (QAE Hw.). The resonance lifetimes (ps) are also listed

State	LAPACK	QAE Cl.	QAE Hw.
Bound E	−32.16 + i0.003	−31.87 + i0.003	−31.51 + i0.003
Resonance E	6.76 − i0.102	7.05 − i0.108	7.75 − i0.097

Resonance τ	26.0	24.5	27.3

There are a number of points about the QAE that are worth discussing. As it was mentioned in the methodology section, we cannot afford the second power of the normalization constraint and, because of that, we had to change the form of the constraint to linear. In a sense, this means that the correct value of the norm, unity, is approached from a single side, from zero to one, and nothing is preventing it from exceeding unity. With a full two-sided (quadratic) constraint, the minimum of the QUBO $F(v)$ will be the minimum of the expectation value part (v, Av), for some reasonable λ. For the one-sided constraint that we use, the two minima diverge, the QUBO minimum diverge further and further from the expectation value minimum as λ increases (the excessive norm drives the solution away). In this case, we have to use the expectation value and the solution type (trivial or non-trivial) to guide the choice of λ and avoid following the QUBO minimum as λ increases. However, λ is not known for the full (quadratic) constraint either and therefore requires searching as well. Thus, both forms of the normalization constraint (linear and quadratic) are practicality the same, as both require λ -searching. However, the one-sided constraint has an advantage of being linear (and therefore quadratic in q) and thus programmable on the D-Wave annealer.

Specifically for quantum scattering problems, the imaginary part of the energy has to be negative, because the physical state width is always a positive number. This means that we do not need the qubit that is responsible for the sign of the imaginary part of eigenvector element. Thus, we can probably save n qubits for this particular class of problems and this may help to improve the quality of solution.

The QAE energies and lifetimes reported in Tables 1 and 2 are not exactly the same as those computed using LAPACK. We found that the *qbsolv* software, that is used to divide large QUBO problems into smaller ones, is noisy and causes discrepancies in energies and lifetimes. More details and possible ways to improve the accuracy can be found in the original QAE paper.[17]

The addition of the Hermitian cross-terms (*i.e.*, the coupling between the real and imaginary components $X(c)$) as an additional constraint in the complex symmetric QAE might be improved upon. The choice of this constraint was motivated by the Hermitian expression but other forms for this constraint might be derived and investigated which could lead to more accurate solutions.

Finally, the method is limited by the number of fully-connected qubits. It uses as many of those as are available (only 64 on the D-Wave 2000Q) which are realized as chains of loosely-connected physical qubits. The lack of full connectivity is compensated classically by the qbsolv interface which effectively boosts the number of fully-connected qubits by two orders of magnitude. As a consequence, for a typical level of discretization $K = 10$ used in the present work for the real and imaginary parts, the largest complex matrix that can probably be targeted is about 300×300, or a diatomic molecule. This estimate is very approximate and should be taken with caution. While the upcoming D-Wave Advantage will have 5k qubits and better connectivity, it is hard to tell if resonances in a triatomic molecule could be computed reliably. The classical part of the QAE (constructing the matrix and submitting QUBOs) has negligible resource requirements.

4 Conclusions

In the present work, we generalized the Quantum Annealer Eigensolver to the complex Hermitian and complex symmetric matrices. The Hermitian case is fundamentally very similar to the real case, since the imaginary terms in the underlying QUBO expression completely cancel out. Thus, the problem is solvable on D-Wave annealers as in the real case. In the complex symmetric case, the imaginary part does not vanish and is treated as another real valued constraint in the QUBO. Since the bound states have zero width (*i.e.*, their eigenvalues are purely real) and the quasi-bound (shape resonance) states also have small widths that increase with increasing resonance energy, we constrain the imaginary part of the QUBO to be of small magnitude. The complex symmetric case also requires yet another constraint between the real and imaginary components in order to maintain stability and converge to a reasonable solution. The Hermitian QUBO provides motivation for a natural choice for this constraint but other possibilities could exist.

Using the newly developed complex QAE extensions, a few ro-vibrational states of molecular oxygen O_2 were calculated in a model 1D potential including a centrifugal component with $j = 6$. The Hermitian QAE gives only real energies, whereas the complex symmetric QAE gives complex eigenvalues which include both the energy and width. All of the bound and resonance state properties, *i.e.* energies, lifetimes and wave functions, were reproduced by the QAE quite well. The D-Wave 2000Q and *qbsolv* software were used to solve the underlying QUBO problems. In principle, the method can be easily extended to molecules with multiple degrees of freedom by constructing a Hamiltonian matrix in a direct-product or any other optimal basis set and using exactly the same QAE methodology to solve the matrix on an annealer.[17] This, however, would require very substantial quantum resources.

This first-ever treatment of scattering resonances on a quantum annealer opens the door to the calculation of rate coefficients of chemical reactions that proceed through formation of long-lived intermediate species, described in quantum mechanics by scattering resonances, and the modeling of chemical dynamics on quantum annealers. We hope that this work will help stimulate additional studies in this fascinating new computational paradigm.

Conflicts of interest

There are no conflicts to declare.

Appendix

This appendix gives detailed QUBO expressions for the real, Hermitian and complex symmetric input matrices.

Real matrix QUBO

We approximate each vector element v_α with a finite number of qubits q_k^α ($1 \leq k \leq K$) using a fixed-point representation:

$$v_\alpha = \sum_{k=1}^{K-1} 2^{k-K} q_k^\alpha - q_K^\alpha \in [-1; 1) \tag{10}$$

As a result, the $F(v)$ function is approximated by

$$F_Q(q) = \sum_{\alpha,\beta}^{n,n} v_\alpha \left(A_{\alpha,\beta} + \lambda \delta_{\alpha,\beta} \right) v_\beta = \sum_{\alpha,k;\beta,l}^{n,K;n,K} Q_{\alpha,k;\beta l} q_k^\alpha q_l^\beta, \tag{11}$$

where the QUBO matrix element is defined as

$$Q_{\alpha,k;\beta,l} = \left(A_{\alpha,\beta} + \lambda \delta_{\alpha,\beta} \right) \times 2^{k+l-2K} (-1)^{\delta_{k,K}+\delta_{l,K}} \tag{12}$$

Thus, in order to obtain a QUBO element, an element of the input matrix A, with λ added to the diagonal, has to be multiplied by the appropriate power of two with the correct sign. Most of the QUBO elements are positive, except those that have either k or l equal to K (but not both simultaneously). The expression for Q in eqn (12) is symmetric with respect to the exchange $\alpha, k \Leftrightarrow \beta, l$ pairs of indices which is a property of any QUBO problem.

Complex QUBO elements

Since the eigenvectors of a complex matrix A are complex, we have to introduce separate real c_α^{Re} and imaginary c_α^{Im} parts of an eigenvector element c_α. The λ -normalization constraint does not change, so we can introduce a complex matrix $Z = A + \lambda I$ for convenience. The objective function that we want to minimize becomes

$$F(c) = \sum_{\alpha,\beta}^{n,n} \bar{c}_\alpha Z_{\alpha,\beta} c_\beta, \tag{13}$$

where the bar above c_α is complex conjugation. A single term of the sum is a complex number

$$\bar{c}_\alpha Z_{\alpha,\beta} c_\beta = \left(Z_{\alpha\beta}^{Re} + iZ_{\alpha\beta}^{Im} \right) c_\alpha^{Re} c_\beta^{Re} + \left(iZ_{\alpha\beta}^{Re} - Z_{\alpha\beta}^{Im} \right) c_\alpha^{Re} c_\beta^{Im} + \left(Z_{\alpha\beta}^{Im} - iZ_{\alpha\beta}^{Re} \right) c_\alpha^{Im} c_\beta^{Re} \tag{14}$$
$$+ \left(Z_{\alpha\beta}^{Re} + iZ_{\alpha\beta}^{Im} \right) c_\alpha^{Im} c_\beta^{Im}$$

Next, we will see what happens to the sum of the (α, β) and (β, α) terms, when the matrix A is Hermitian or complex symmetric.

Hermitian matrix QUBO.

Because $Z_{\alpha\beta} = \bar{Z}_{\beta\alpha}$ for the Hermitian matrix A, the sum of two opposite (α, β) and (β, α) terms of the objective function $F(c)$ is a real number

$$\bar{c}_\alpha Z_{\alpha\beta} c_\beta + \bar{c}_\beta Z_{\beta\alpha} c_\alpha = 2Z_{\alpha\beta}^{Re} c_\alpha^{Re} c_\beta^{Re} - 2Z_{\alpha\beta}^{Im} c_\alpha^{Re} c_\beta^{Im} \tag{15}$$
$$+ 2Z_{\alpha\beta}^{Im} c_\alpha^{Im} c_\beta^{Re} + 2Z_{\alpha\beta}^{Re} c_\alpha^{Im} c_\beta^{Im}$$
$$= 2\text{Re}\left(\bar{c}_\alpha Z_{\alpha\beta} c_\beta \right)$$

Thus, for a Hermitian matrix the eigenvectors are complex but the QUBO expression is purely real, due to the cancellation of the imaginary part in the sum over the (α, β) and (β, α) terms. This is consistent with the property that eigenvalues of a Hermitian matrix are real.

Although the sum has reduced to the simple form of $\text{Re}((\alpha, \beta))$, all four terms in eqn (15) have to be added to the QUBO, with both c_α^{Re} and c_α^{Im} discretized as in the real symmetric case (eqn (10)–(12)). We note that by using the four terms in eqn (15), the sums over α and β in constructing the functional $F(c)$ in eqn (13) are now restricted to $\alpha = 1, 2, \dots n$ with $\beta \geq \alpha$.

Complex symmetric matrix QUBO.
For the complex symmetric case, $Z_{\alpha\beta} = Z_{\beta\alpha}$. In contrast to the Hermitian case, the sum of (α, β) and (β, α) terms in the QUBO is a complex number

$$
\begin{aligned}
\bar{c}_\alpha Z_{\alpha\beta} c_\beta + \bar{c}_\beta Z_{\beta\alpha} c_\alpha &= Z_{\alpha\beta}(\bar{c}_\alpha c_\beta + \bar{c}_\beta c_\alpha) \\
&= 2Z_{\alpha\beta}(c_\alpha^{\text{Re}} c_\beta^{\text{Re}} + c_\alpha^{\text{Im}} c_\beta^{\text{Im}}) \\
&= 2Z_{\alpha\beta}^{\text{Re}} c_\alpha^{\text{Re}} c_\beta^{\text{Re}} + 2Z_{\alpha\beta}^{\text{Im}} c_\alpha^{\text{Re}} c_\beta^{\text{Re}} \times i \\
&\quad + 2Z_{\alpha\beta}^{\text{Im}} c_\alpha^{\text{Im}} c_\beta^{\text{Im}} \times i + 2Z_{\alpha\beta}^{\text{Re}} c_\alpha^{\text{Im}} c_\beta^{\text{Im}}
\end{aligned}
\tag{16}
$$

The first and fourth terms in eqn (16) are identical to those in eqn (15), but the second and third terms are different and now imaginary. Thus, in the complex symmetric case the sum of (α, β) and (β, α) does not reduce to a real number. This presents a problem, since the QUBO function has to be real. To overcome this, we treat the imaginary terms as real and include them in the functional as a second constraint $(-2E^{\text{Im}})$ which must be minimized along with the expectation value and normalization constraint (see eqn (6) in the main text)

$$
-2E_{\alpha\beta}^{\text{Im}} = 2Z_{\alpha\beta}^{\text{Im}} c_\alpha^{\text{Re}} c_\beta^{\text{Re}} + 2Z_{\alpha\beta}^{\text{Im}} c_\alpha^{\text{Im}} c_\beta^{\text{Im}}
\tag{17}
$$

We also note that there is no coupling (cross terms) between the real c^{Re} and imaginary c^{Im} in eqn (16) in contrast to eqn (15), which leads to stability issues. To overcome this problem, a third constraint $-X(c)$ (see eqn (6)) is added to the QUBO. The pairwise terms of $-X(c)$ are the cross terms from eqn (15)

$$
-X_{\alpha\beta}(c) = -2Z_{\alpha\beta}^{\text{Im}} c_\alpha^{\text{Re}} c_\beta^{\text{Im}} + 2Z_{\alpha\beta}^{\text{Im}} c_\alpha^{\text{Im}} c_\beta^{\text{Re}}
\tag{18}
$$

The role of the $-X(c)$ constraint becomes clear, once one recognizes the cross product between the c_α and c_β, represented as vectors on the complex plane (with $x = \text{Re}$ and $y = \text{Im}$)

$$
-X_{\alpha\beta}(c) = -2Z_{\alpha\beta}^{\text{Im}} |c_\alpha||c_\beta| \sin(\theta_{\alpha\beta}),
\tag{19}
$$

where $|c_\alpha|$ and $|c_\beta|$ are vector magnitudes and $\theta_{\alpha\beta}$ is the relative angle between the vectors. Thus, the $-X(c)$ constraint is a weighted sum of pairwise terms, which encourages the optimization to explore regions away from $\sin(\theta_{\alpha\beta}) = 0$ (*i.e.,* to explore the full 2π range in $\theta_{\alpha\beta}$) similar to the normalization

constraint which encourages solutions with non-zero norm. Without this "angular repulsion" between the vector elements, the optimization collapses to $\theta_{\alpha\beta} = 0$ and does not explore the full 2π range of possibilities. It therefore never converges to a solution and/or becomes unstable. The normalization constraint separately encourages non-zero $|c_\alpha|$ and $|c_\beta|$. Again, all the sums over α and β are restricted to $\alpha = 1,2,\ldots n$ with $\beta \geq \alpha$.

D-Wave setup

The D-Wave 2000Q was accessed using the D-Wave's Ocean tools. Since in an actual quantum annealer some qubits and couplers are not active (unrepresented), we have been using the Virtual Full-Yield Chimera (VFYC) version of a hardware QUBO solver, which postprocess a QUBO solution to fix unrepresented qubits and couplers. This allows for the development of a "portable" code. The embedding (mapping QUBO variables to qubits) was done automatically based on Ocean's heuristic algorithms, and the default annealing schedule was employed.

Acknowledgements

Notes and references

T. D. Ladd, F. Jelezko, R. Laflamme, Y. Nakamura, C. Monroe and J. L. O'Brien, *Nature*, 2010, **464**, 45

L. Gyongyosi and S. Imre, *Comput. Sci. Rev.*, 2019, **31**, 51–71

A. O. Pittenger, *An introduction to quantum computing algorithms*, Springer Science & Business Media, 2012, vol. 19

A. Montanaro, *npj Quantum Information*, 2016, **2**, 1–8

J. Preskill, *Quantum*, 2018, **2**, 79

I. Kassal, J. D. Whitfield, A. Perdomo-Ortiz, M.-H. Yung and A. Aspuru-Guzik, *Annu. Rev. Phys. Chem.*, 2011, **62**, 185–207

Y. Cao, J. Romero, J. P. Olson, M. Degroote, P. D. Johnson, K. Máia, I. D. Kivlichan, T. Menke, B. Peropadre, N. P. D. Sawaya, S. Sim, L. Veis and A. Aspuru-Guzik, *Chem. Rev.*, 2019, **119**, 10856–10915

S. McArdle, S. Endo, A. Aspuru-Guzik, S. C. Benjamin and X. Yuan, *Rev. Mod. Phys.*, 2020, **92**, 015003

A. Peruzzo, J. McClean, P. Shadbolt, M.-H. Yung, X.-Q. Zhou, P. J. Love, A. Aspuru-Guzik and J. L. O'Brien, *Nat. Commun.*, 2014, **5**, 4213

J. R. McClean, J. Romero, R. Babbush and A. Aspuru-Guzik, *New J. Phys.*, 2016, **18**, 023023

P. J. J. O'Malley, R. Babbush, I. D. Kivlichan, J. Romero, J. R. McClean, R. Barends, J. Kelly, P. Roushan, A. Tranter, N. Ding, B. Campbell, Y. Chen, Z. Chen, B. Chiaro, A. Dunsworth, A. G. Fowler, E. Jeffrey, E. Lucero, A. Megrant, J. Y. Mutus, M. Neeley, C. Neill, C. Quintana, D. Sank, A. Vainsencher, J. Wenner, T. C. White, P. V. Coveney, P. J. Love, H. Neven, A. Aspuru-Guzik and J. M. Martinis, *Phys. Rev. X*, 2016, **6**, 031007

D-Wave Systems Inc., QPU Properties: D-Wave 2000Q Online System (DW_2000Q_3), 09-1180A-A, 2018.

A. Mizel, D. A. Lidar and M. Mitchell, *Phys. Rev. Lett.*, 2007, **99**, 070502

R. Xia, T. Bian and S. Kais, *J. Phys. Chem. B*, 2017, **122**, 3384–3395

M. Streif, F. Neukart and M. Leib, International Workshop on Quantum Technology and Optimization Problems, 2019, pp. 111-122.

S. N. Genin, I. G. Ryabinkin and A. F. Izmaylov, arXiv preprint arXiv:1901.04715, 2019.

A. Teplukhin, B. K. Kendrick and D. Babikov, *J. Chem. Theory Comput.*, 2019, **15**, 4555–4563

P. Hauke, H. G. Katzgraber, W. Lechner, H. Nishimori and W. D. Oliver, *Rep. Prog. Phys.*, 2020, **83**, 054401

E. Anderson, Z. Bai, C. Bischof, S. Blackford, J. Demmel, J. Dongarra, J. Du Croz, A. Greenbaum, S. Hammarling, A. McKenney and D. Sorensen, *LAPACK Users' Guide, Society for Industrial and Applied Mathematics*, Philadelphia, PA, 3rd edn, 1999

P. Echenique and J. L. Alonso, *Mol. Phys.*, 2007, **105**, 3057–3098

M. Booth, S. Reinhardt and A. Roy, Partitioning optimization problems for hybrid classcal/quantum execution, 2017, Technical Report, 14-1006A-A, http://www.dwavesys.com.

S. Kais and D. Herschbach, *J. Chem. Phys.*, 1993, **98**, 3990–3998

A. U. Maheswari, P. Prema, S. Mahadevan and C. Shastry, *Pramana*, 2009, **73**, 969